A Novel Method for Capacity Fade Analysis of Lithium-ion Batteries Based on Multi-Physics Model

Liqiang Zhang,
College of Engineering
Ocean University of China
Qingdao 266100, China
zhang.lq@ouc.edu.cn

Junfu Li, Chao Lyu
School of Electrical Engineering and Automation
Harbin Institute of Technology
Harbin 150001, China

***Abstract*—Detailed information of the capacity fade mechanisms can be very beneficial for the prognostics and health management (PHM) study of lithium-ion batteries. This paper reports a novel capacity fade analysis method. The parameter degradation of multi-physics model is achieved, and the three main factors of capacity fade is quantitatively calculated by using the obtained parameters. The results show that the loss of active material and the loss of Li inventory is the main reason of capacity fade at high temperature and room temperature, respectively. And the proposed method can further help improving battery (pack) management, reliability and safety.**

Keywords- degradation analysis; capacity fade; multi-physics model; parameter identification; lithium-ion battery

I. INTRODUCTION

Lithium-ion battery is a typical dynamic and nonlinear electrochemical system. Lack of detailed description of capacity degradation mechanisms is the main limitation of accurate health evaluation and prognostic. The key issue is the way to extract the capacity degradation mechanisms non-destructively.

There are two non-destructive methods for analyzing the mechanisms of capacity fade of Lithium-ion batteries. One is based on voltage curves, in [1-3] the incremental capacity (IC or dQ/dV) and differential voltage (DV or dV/dQ) analysis are used and they can be also used to yield a quantitative assessment of different degradation mode via a diagnostic and prognostic model. The other one is to analyze the electrochemical mechanisms using identified model parameters. In [4-6], the stoichiometric numbers of the electrode material were used to indicate the stages of capacity fade. A.P. Schmidt *et al*. investigated the relationship between the volume fraction of active material in the electrode (ε_s), the ionic conductivity of the electrolyte (κ_e) and the cycle number during aging, and used them as characteristics to evaluate the state of health (SOH) of batteries[7]. R. Fu *et al*. treated some parameters of an electrochemical thermal model as degradation parameters to analyze the degradation effects considering side reactions, including the volume fraction of active material in the electrode, the solid electrolyte interface (SEI) resistance (R_{film}) and the diffusion coefficient of electrolyte (D_e)[8]. These papers investigated the degradation laws of some parameters, and some fundamental mechanisms can be acquired, but the quantitative relation between parameter degradation and capacity fade is still absent.

This paper introduces a novel method for capacity degradation analysis using physics-based model, and the model parameters are used to calculate the factors of capacity fade quantitatively. The remainder of this paper is organized as follows: Section 2 provides the multi-physics model of lithium-ion battery; Section 3 summaries the experimental setup; Section 4 proposes a novel method for decomposition of capacity loss; and Section 5 presents the results and discussion. Conclusions of this paper are presented in the final section.

II. MULTI-PHYSICS MODEL

The multi-physics model consists three parts: the electrochemical model, the thermal model and the radial heat distribution model:

The Electrochemical part is described by P2D model[9-10]. Section B-B in Fig. 1 shows the schematic of the P2D model for a lithium-ion battery. It consists of two current collectors, a negative electrode (anode), a separator and a positive electrode (cathode). All electrodes and separator have porous structures. Two inner boundaries and two external boundaries are also shown. The physical and chemical processes such as ion diffusion, migration, transportation and electrochemical kinetics are described by several partial differential equations and algebraic equations in TABLE I.

In (6), E_{ocv} is the equilibrium potential, which is a function of the solid phase Li^+ concentration at the particle surface. The E_{ocv} of Li_xC_6 and Li_yCoO_2 anode are obtained from [11] and [12], respectively.

Thermal phenomena such as energy conservation, heat generation and exchange also occur during the charge/discharge process, and they can be simulated by the P2D model, as presented in TABLE II. The heat generation occurs in the spiral roll, including the heat of electrochemical reactions, entropic heat and ohmic heating. Heat exchange, including convection and radiation, only occurs at the surface of the cylindrical battery.

Some parameters in the P2D model—such as solid phase diffusion coefficients $D_{s,a}$ and $D_{s,c}$, solution phase conductivity κ_e, solution phase diffusion coefficient D_e and electrochemical

978-1-5090-0382-2/16/$31.00 ©2015 IEEE

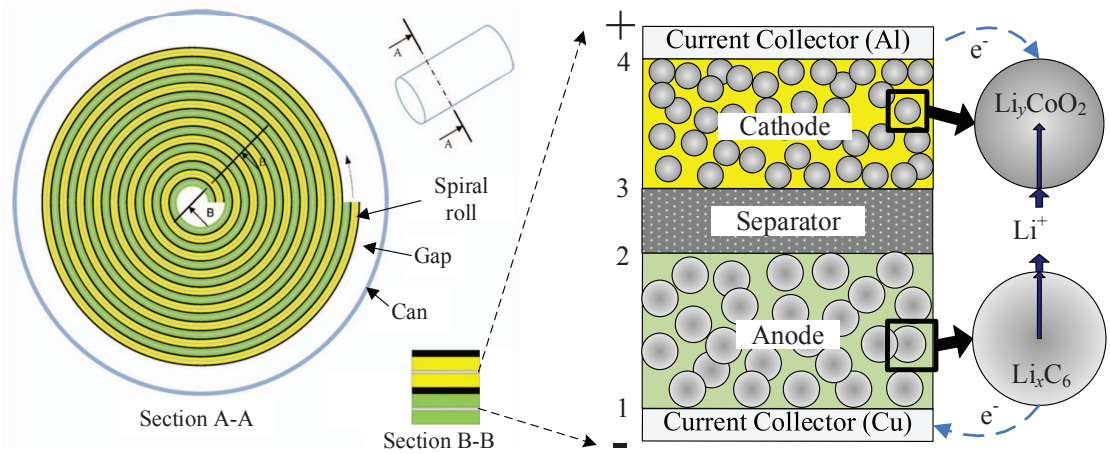

Figure 1. Schematic of the multi-physics model.

TABLE I. GOVERNING EQUATIONS AND BOUNDARY CONDITIONS OF THE P2D MODEL.

Mechanisms	Equation	Eq.	Boundary condition
Solid phase diffusion	$\frac{\partial C_s}{\partial t}=\frac{1}{r^2}\nabla\cdot(D_s r^2\nabla C_s)$	(1)	$\left.\frac{\partial C_s}{\partial r}\right\|_{r=R_s}=-\frac{j_{Li}}{D_s}$, $\left.\frac{\partial C_s}{\partial r}\right\|_{r=0}=0$
Electrolyte phase diffusion	$\varepsilon_e\frac{\partial C_e}{\partial t}=\nabla\cdot(D_e^{eff}\nabla C_e)+\frac{a_s}{F}(1-t_+^0)\cdot i_s$	(2)	$\left.\frac{\partial C_e}{\partial x}\right\|_1=\left.\frac{\partial C_e}{\partial x}\right\|_4=0$, $-D_{e,a}^{eff}\left.\frac{\partial C_e}{\partial x}\right\|_{2^-}=-D_{e,s}^{eff}\left.\frac{\partial C_e}{\partial x}\right\|_{2^+}$, $-D_{e,s}^{eff}\left.\frac{\partial C_e}{\partial x}\right\|_{3^-}=-D_{e,c}^{eff}\left.\frac{\partial C_e}{\partial x}\right\|_{3^+}$
Solid phase charge balance	$i_1=-\sigma_s^{eff}\nabla\phi_s$	(3)	$\left.\frac{\partial\phi_s}{\partial x}\right\|_{2^-}=\left.\frac{\partial\phi_s}{\partial x}\right\|_{3^+}=0$, $\phi_s\|_1=0$, $\left.\frac{\partial\phi_s}{\partial x}\right\|_4=-\frac{i}{\sigma_{s,a}^{eff}}$
Electrolyte phase charge balance	$i_2=-\kappa_e^{eff}\nabla\phi_e+\frac{2\kappa_e^{eff}RT}{F}(1+\frac{\partial\ln f_\pm}{\partial\ln C_e})(1-t_+^0)\nabla\ln C_e$	(4)	$\left.\frac{\partial\phi_e}{\partial x}\right\|_1=\left.\frac{\partial\phi_e}{\partial x}\right\|_4=0$, $\phi_e\|_{2^-}=\phi_e\|_{2^+}$, $\phi_e\|_{3^-}=\phi_e\|_{3^+}$
Electrochemical kinetics (Butler–Volmer equation)	$i_s=nFj_{Li}=i_0[\exp(\frac{\alpha_a F}{RT}\eta)-\exp(-\frac{\alpha_c F}{RT}\eta)]$	(5)	
Reaction overpotential	$\eta=\phi_s-\phi_e-E_{ocv}-i_s R_{film}$	(6)	
Exchange current density	$i_0=k_s C_e^{\alpha_a}(C_{s,MAX}-C_{e/s})^{\alpha_a}C_{e/s}^{\alpha_c}$	(7)	
Terminal voltage of the battery	$U_{app}=\phi_s\|_4-\phi_s\|_1-iR_{ext}$	(8)	

reaction rate $k_{s,a}$ and $k_{s,c}$—are coupled with the battery temperature. These parameters can be updated by the Arrhenius law. In (15), X_i represents the parameters mentioned above, $X_{i,ref}$ is the parameter value at reference temperature T_{ref}, E_i denotes the corresponding activation energy of parameter X_i, respectively. In addition, the equilibrium potential depends on battery temperature according to the Nernst equation. An electrochemical-thermal coupled model is presented by feeding back the relationship between temperature dependent

TABLE II. EQUATIONS OF THE THERMAL MODEL.

Mechanisms	Equation	Eq.
Energy balance	$\rho C_p \frac{\partial T}{\partial t} = -\nabla(\lambda \nabla T) + \dot{Q}$	(9)
Electrochemical reaction heat	$\dot{Q}_{rea} = a_s i_s (\phi_s - \phi_e - E_{ocv})$	(10)
Entropic heat	$\dot{Q}_{ent} = a_s i_s T \frac{dE_{ocv}}{dT}$	(11)
Ohmic heat	$\begin{cases} \dot{Q}_{ohm,s} = \sigma_s^{eff} \nabla\phi_s \nabla\phi_s \\ \dot{Q}_{ohm,e} = \kappa_e^{eff} \nabla\phi_e \nabla\phi_e \\ \quad + \kappa_e^{D,eff} \nabla \ln C_e \nabla\phi_e \\ \dot{Q}_{ext} = i_{app}^2 R_{ext} / L \end{cases}$	(12)
Heat exchange (convection)	$\dot{q}_c = h(T_{sh} - T_{am})$	(13)
Heat exchange (radiation)	$\dot{q}_r = \varepsilon\sigma(T_{sh}^4 - T_{am}^4)$	(14)
Arrhenius' law	$X_i = X_{i,ref} \exp[\frac{\bar{E}_i}{R}(\frac{1}{T_{ref}} - \frac{1}{T})]$	(15)
Nernst equation	$E_{ocv} = E_{ocv}^{ref} + (T - T_{ref}) \frac{dE_{ocv}}{dT}$	(16)

parameters and thermal effects to the P2D model. In (11) and (16), $\frac{dE_{ocv}}{dT}$ is the entropy coefficient, obtained from [11].

The temperature distribution in the radial direction of a cylindrical battery is more obvious than that in the axial direction due to the small thermal conductivity[13]. So, the heat conduction term in (9) can be expressed in one-dimensional by Fourier's Law:

$$-\nabla(\lambda_r \nabla T) = \lambda_r (\frac{\partial^2 T}{\partial R^2} + \frac{1}{R}\frac{\partial T}{\partial R}) \tag{17}$$

A thermal impedance model is used to simulate the thermal distribution in the radial direction of cylindrical lithium-ion batteries, details seen in our previous work[12, 14]. The terminal voltage U_{app} and shell temperature T_{sh} can be obtained accurately, and all parameters in this first principle model have clear physical significances. So, the parameters acquired during aging test can indicate the internal status of the batteries, and the aging mechanisms can be analyzed by using them.

III. EXPERIMENTS

For aging investigation, cylindrical batteries manufactured by DLG Power Battery (Shanghai, China), labeled ICR14500E-075 have been used. The batteries are designed for mobile devices and have a capacity of 750mAh. Cycle Aging Test (CAT) and Reference Performance Test (RPT) were conducted alternately, and the test schedule is shown in Fig. 2. Experimental U_{app} and T_{sh} data was acquired by a Battery Testing System (Neware BTS-5V-6A, China) every 10s. In CAT, the constant current is set to 1C and 2C, the ambient temperature is set to RT=25℃ and HT=50℃, so there are four aging patterns denoted by HT 2C, HT 1C, RT 2C and RT 1C. And the ambient temperature was controlled by a high-precision thermal chamber (Partner PTC14003-M, China) in both CAT and RPT.

The current profiles of dynamic charge/discharge and experimental data of U_{app} and T_{sh} in RPT at 15℃ and 30℃ are shown as Fig. 3, measured data will be used for parameter identification. And the experimental data of 0.5C discharge at 25℃ will be used for tracking the capacity fade, as shown in Fig. 4.

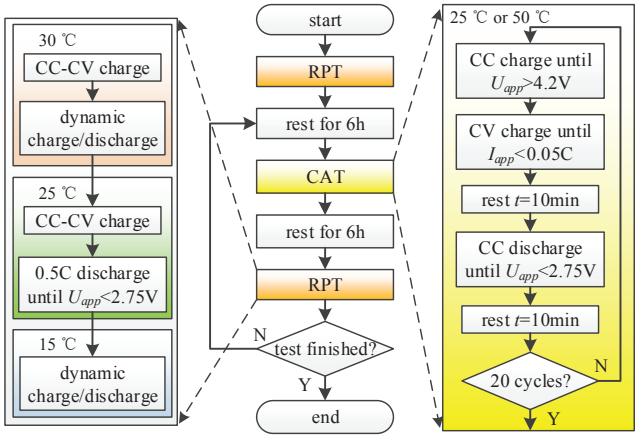

Figure 2. Flow chart of the CAT and RPT schedule.

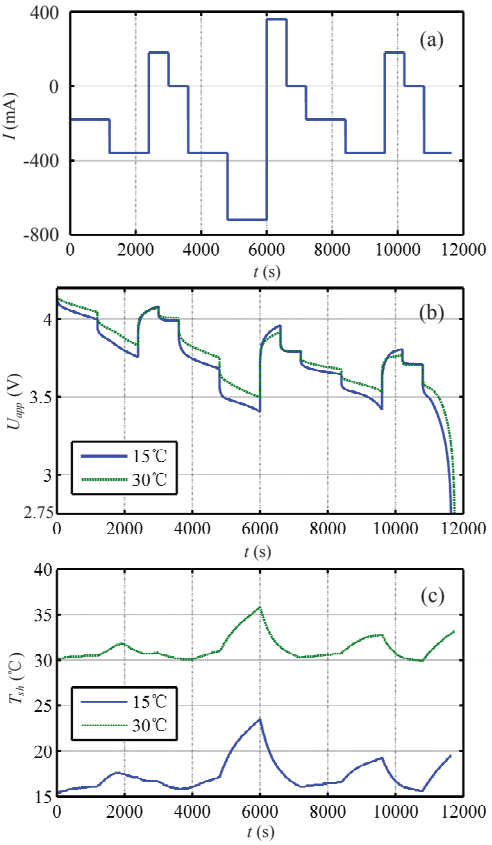

Figure 3. Current profile and experimental data of U_{app} and T_{sh} in RPT

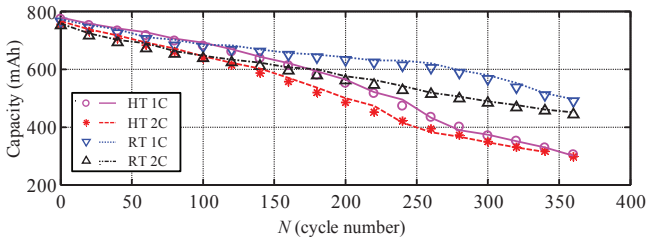

Figure 4. Simulated data and experimental capacity loss under different aging patterns

The parallelized Multi-Objective Genetic Algorithm (MOGA)[15-16] were used for parameter identification. The four objective functions are defined as the Sum of Squared Error (SSE) between the model outputs and the experimental data of RPT at 15 ℃ and 30 ℃:

$$\text{minimize}\begin{cases} ObjF_1 = \sum_{i=1}^{N}(U_{app,i,15℃}-\hat{U}_{app,i,15℃})^2 \\ ObjF_2 = \sum_{i=1}^{N}(T_{sh,i,15℃}-\hat{T}_{sh,i,15℃})^2 \\ ObjF_3 = \sum_{i=1}^{N}(U_{app,i,30℃}-\hat{U}_{app,i,30℃})^2 \\ ObjF_4 = \sum_{i=1}^{N}(T_{sh,i,30℃}-\hat{T}_{sh,i,30℃})^2 \end{cases} \tag{18}$$

where $U_{app,i}$ is the model output terminal voltage data, the $\hat{U}_{app,i}$ and $\hat{T}_{sh,i}$ is the experimental data, N is the number of data points. The optimal solution of identification problem is a set of parameters, with which the model simulated data should fit the experimental data best. Therefore, the degradation of all parameters under four ageing patterns can be obtained.

IV. Analysis of Capacity Fade

A. Factors of capacity fade

Theoretically, the total capacity of the active material is determined by:

$$\begin{cases} Cap_a^{total} = A_{cell}h_a\varepsilon_{s,a}M_a\rho_a \\ Cap_c^{total} = A_{cell}h_c\varepsilon_{s,c}M_c\rho_c \end{cases} \tag{19}$$

Cap^{total} is the total capacity an electrode contains when the lithium-ions fully insert/deinsert into/from the active materials. The constants in (19) are listed in TABLE III, so the total capacity is only determined by the volume fraction of active material (ε_s).

In fact, the lithium-ions do not fully insert/deinsert into/from the active materials, the stoichiometric number changes in a certain range, which is defined as the stoichiometric windows, and expressed by Δx and Δy:

TABLE III. Geometrical and Material Parameters in (19).

Parameter	Description	Anode	Cathode
A_{cell} (m^2)	Area of the electrode	0.0284	0.0284
L (m)	Thinkness of the electrode	7.2e^{-5}	6.1e^{-5}
M (mAh/g)	Coulombic capacity	372	274
ρ (kg/m3)	Density	2260	5010

$$\begin{cases} \Delta x = \dfrac{Capacity}{Cap_a^{total}} = x_0 - x_{end} \\ \Delta y = \dfrac{Capacity}{Cap_c^{total}} = y_{end} - y_0 \end{cases} \tag{20}$$

where x_0 and y_0 are respectively the stoichiometric numbers of anode and cathode when the battery is fully charged, while x_{end} and y_{end} are the stoichiometric numbers when the battery is fully discharged. So the actual cycle capacity of the battery is determined by two factors: the volume fraction of active material (ε_s) and the stoichiometric windows (Δx and Δy).

By the mentioned method in Seciton III, the values of parameter $\varepsilon_{s,a}$, $\varepsilon_{s,c}$ in (19) and x_0, y_0 in (20) during the degradation under different aging patterns were acquired. Besides, x_{end} and y_{end} can be calculated using the obtained parameters by using (20), Fig. 5 presents the degradations of stoichiometric numbers under different aging patterns.

According to (19), the degradation of parameter ε_s causes active material loss, and this part of capacity loss is defined as "loss of active material (LAM)". According to (20), actual discharge capacity will be lost when the stoichiometric windows decrease, and this part can be defined as "loss of Li inventory (LLI)".

Some conclusions can be drawn from Fig. 5:

1) From the position of x_{end} and y_{end}, the anode and the cathode are both the control electrodes in the early stage of aging (0~120 cycles), means that the voltage drop of whole battery is caused by cathode potential drop and anode potential rise. But in the later stage, only the anode is the control electrode, means that voltage drop of the whole battery is only caused by the anode potential rise.

2) Since the x_{end} rises during aging while the cathode potential y_{end} stays on the voltage plateau, so the open circuit potential at discharge ending $E_{ocv}^{eq} = E_{ocv,c}(y_{end}) - E_{ocv,a}(x_{end})$ rises, considering that the discharge cut-off voltage remains U_{app}=2.75V, thus the total overpotential rises. In the late stage of HT aging, x_{end} is approximately equal to 0.05~0.06, shows that there are some lithium-ion have not been used yet when the terminal voltage of the battery reach the cut-off voltage. So, another factor of capacity fade is the incomplete discharge caused by overpotential, defined as "under discharge (UD)".

B. Decomposition of capacity fade factors

For anode, the capacity of the N^{th} cycle can be obtained from (20):

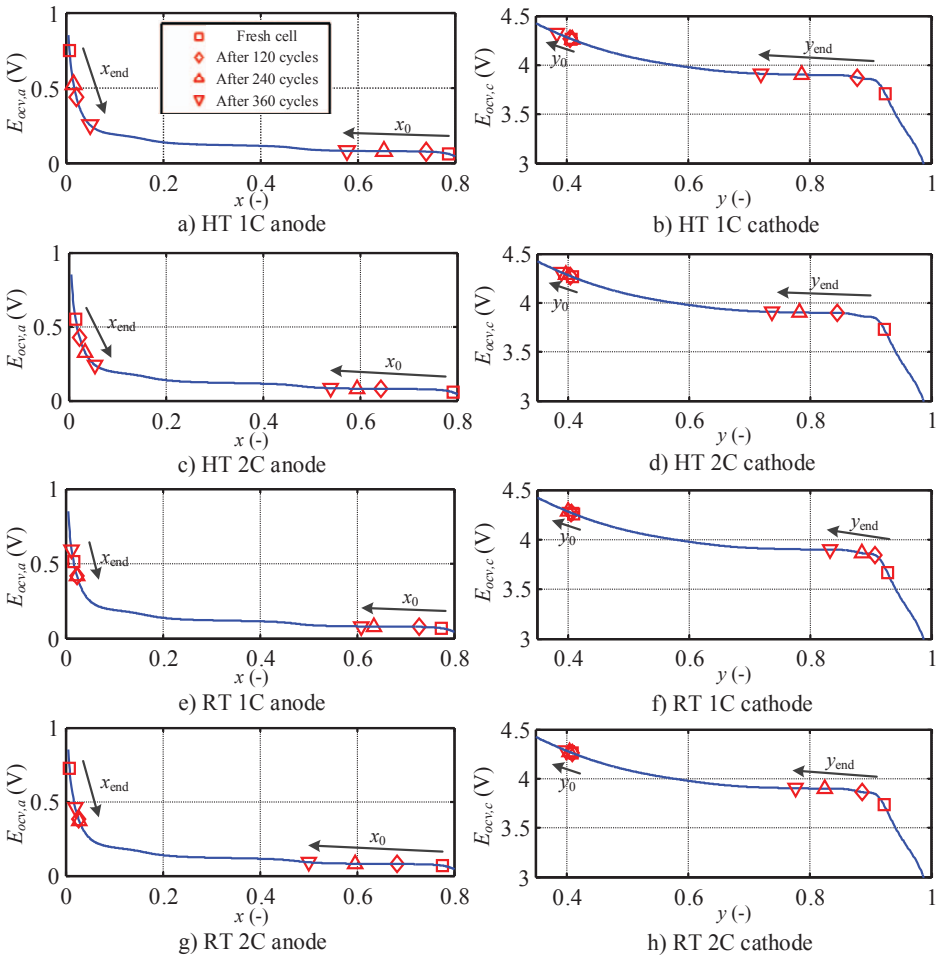

Figure 5. Degradations of the stoichiometric numbers under different aging patterns

$$\begin{aligned} Cap(N) &= \Delta x(N)\cdot Cap_a^{total}(N) \\ &= \left[x_0(N) - x_{end}(N)\right]\cdot Cap_a^{total}(N) \end{aligned} \tag{21}$$

Compare to a fresh cell (N=0), the capacity loss after N cycles can be calculated as:

$$\begin{aligned} Cap_{loss}(N) &= Cap(0) - Cap(N) \\ &= \Delta x(0)\cdot Cap_a^{total}(0) - \Delta x(N)\cdot Cap_a^{total}(N) \end{aligned} \tag{22}$$

Equation (22) can be reformed into:

$$\begin{aligned} Cap_{loss}(N) &= \Delta x(0)\cdot Cap_a^{total}(0) - \Delta x(N)\cdot Cap_a^{total}(N) \\ &\quad -\Delta x(N)\cdot Cap_a^{total}(0) + \Delta x(N)\cdot Cap_a^{total}(0) \\ &= \left[\Delta x(0) - \Delta x(N)\right]\cdot Cap_a^{total}(0) \\ &\quad +\Delta x(N)\cdot\left[Cap_a^{total}(0) - Cap_a^{total}(N)\right] \end{aligned} \tag{23}$$

Since $\left[Cap_a^{total}(0) - Cap_a^{total}(N)\right]$ is the total capacity loss of active material after N^{th} cycle, the actual capacity loss caused by LAM can be obtained by multiplying $\Delta x(N)$. Therefore, the second term of the right side in (23) can be marked as $Cap_{loss}^{LAM}(N)$.

Expanding the first term of the right side in (23), we can obtain:

$$\begin{aligned} Cap_{loss}(N) &= \left[x_0(0) - x_{end}(0) - x_0(N) + x_{end}(N)\right]\cdot Cap_a^{total}(0) \\ &\quad +Cap_{loss}^{LAM}(N) \\ &= \left[x_0(0) - x_0(N)\right]\cdot Cap_a^{total}(0) \quad \cdots\cdots\cdots\cdots ① \\ &\quad +\left[x_{end}(N) - x_{end}(0)\right]\cdot Cap_a^{total}(0) \quad \cdots\cdots\cdots ② \\ &\quad +Cap_{loss}^{LAM}(N) \quad \cdots\cdots\cdots\cdots\cdots\cdots\cdots\cdots ③ \end{aligned} \tag{24}$$

The reason of Δx decrease can be divided into two parts: the x_0 decrease caused by LLI, and the x_{end} increase caused by UD.

Details of LLI part is presented as follows: Assuming that the total quantity of active material remain the same during aging (no LAM), and the total overpotential is stable (no UD), when the battery was cut-off, the parameter x_{end} should be a constant valued, thus the value of parameter x_0 is determined

by the charged capacity. LLI causes the decrease of Δx, so the decrease of x_0 causes capacity loss, and it is regarded as the LLI part.

Details of UD part is presented as follows: Assuming that there is no LAM and UD, the parameter y_{end} should be on the the voltage plateau at the end of discharging process, so the equilibrium potential is totally determined by the parameter x_{end}, and the value of x_{end} should be a constant if the total overpotential remains the same. When UD occurs, the overpotential increases and the potential of anode should decrease, so the value of parameter x_{end} should increase. Therefore, the UD part of capacity fade can be denoted as x_{end} increase.

When the total active material remains stable, the capacity fade causes by the mentioned reasons can be explained using the ① and ② term of the right side in (24), marked as $Cap_{loss}^{LLI}(N)$ and $Cap_{loss}^{UD}(N)$. So, when the anode is the control electrode, the quantitative decomposition of capacity fade factors can be expressed as follows:

$$Cap_{loss}^{LAM}(N) = \Delta x(N) \cdot \left[Cap_a^{total}(0) - Cap_a^{total}(N) \right] \quad (25)$$

as capacity loss caused by LAM.

$$Cap_{loss}^{LLI}(N) = \left[x_0(0) - x_0(N) \right] \cdot Cap_a^{total}(0) \quad (26)$$

as capacity loss caused by LLI.

$$Cap_{loss}^{UD}(N) = \left[x_{end}(N) - x_{end}(0) \right] \cdot Cap_a^{total}(0) \quad (27)$$

as capacity loss caused by UD.

V. Results and Discussion

The three factors of capacity fade can be quantitatively calculated using (25) to (27) with obtained parameters, Fig. 6 shows decomposition results under four different aging patterns. TABLE IV shows the average ratios of different factors of the capacity loss in different stages.

At high temperature (Fig. 6 a) b)), two main steps of capacity fade can be seen. In early-medium stage, the capacity decreases slowly, while in late stage the capacity decreases more rapidly. LAM part increases faster in the late stage, and the ratio is up to 40%, so LAM should be considered as the main factor of capacity fade in late stage. LLI part increases linearly, and in all stages the ratio is never less than 41%, shows that it is another dominant factor of capacity fade.

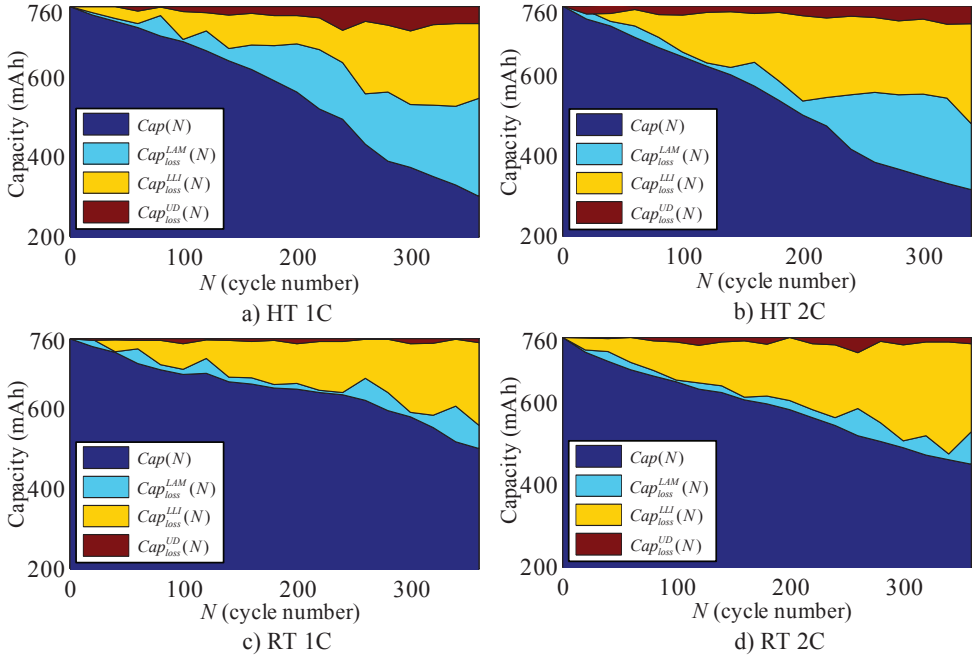

Figure 6. Decomposition of the capacity loss under different aging patterns

TABLE IV. Average ratios of different factors of the capacity loss in different stages

Factors	HT 1C			HT 2C			RT 1C			RT 2C		
	Early	*Medium*	*Late*	*Early*	*Medium*	*Late*	*Early*	*Medium*	*Late*	*Early*	*Medium*	*Late*
LAM	30%	45%	43%	26%	23%	44%	38%	9%	23%	18%	10%	16%
LLI	60%	41%	46%	46%	69%	47%	50%	85%	74%	74%	83%	77%
UD	10%	14%	11%	28%	8%	9%	12%	6%	3%	8%	7%	7%

At room temperature (Fig. 6 c) d)), three main steps of capacity fade can be seen. The capacity decreases rapidly in the early stage, and slowly in medium stage, then rapidly again in the late stage. LAM part increases very slowly, and has very little proportion. While the LLI part increases linearly, the ratio remains more than 50% in all stage. Especially, in medium-late stage, the ratio of LLI is up to 74%, so it is the most important factor of capacity fade.

Above all, in the early stage of aging, the anode and cathode are both control electrodes, LLI causes most capacity loss. And in medium stage, the cathode becomes no longer a control electrode, the capacity fade is caused by LAM at high ambient temperature and LLI in room temperature. By the way, LAM and UD part at high temperature is obviously higher than that at room temperature, showing that more active material is lost and higher overpotential occurred. In addition, higher cycle current rate causes more LLI, and it is the main reason for the rapid capacity lost at the same ambient temperature but different current rates.

VI. Conclusion

A novel capacity fade analysis method is proposed in this paper. The parameter degradation of multi-physics model is achieved, and the three main factors of capacity fade (LAM, LLI and UD) is quantitatively calculated by using the obtained parameters. The results show that, LAM is the dominant factor of capacity fade when the batteries are cycled at high ambient temperature. While, the LLI is the dominant factor at room temperature, and higher current rate will cause more LLI in cycle aging. This proposed method can provide quantitatively decomposition of capacity fade factors non-destructively. The details revealed by this approach provide a more detailed understanding of the degradation than that achieved by just monitoring the capacity and internal resistance of batteries. Both the method and the results of this work can be very beneficial for the PHM study of lithium-ion batteries, and further help improve battery (pack) management, reliability and safety.

Acknowledgment

This research was financially supported by the Fundamental Research Funds for the Central Universities. We are also grateful to all anonymous reviewers for providing useful comments and suggestions that resulted in the improved quality of this paper.

References

[1] M. Dubarry, and B.Y. Liaw, "Identify capacity fading mechanism in a commercial $LiFePO_4$ cell," Journal of Power Sources, vol. 194, pp. 541-549, 2009.

[2] M. Dubarry, C. Truchot, B.Y. Liaw, "Synthesize battery degradation modes via a diagnostic and prognostic model," Journal of Power Sources, vol. 219, pp. 204-216, 2012.

[3] M. Dubarry, C. Truchot, B.Y. Liaw, "Cell degradation in commercial $LiFePO_4$ cells with high-power and high-energy designs," Journal of Power Sources, vol. 258, pp. 408-419, 2014.

[4] Q. Zhang, R.E. White, "Calendar life study of Li-ion pouch cells: Part 2: Simulation," Journal of Power Sources, vol. 179, pp. 785-792, 2008.

[5] Q. Zhang, R.E. White, "Capacity fade analysis of a lithium ion cell," Journal of Power Sources, vol. 179, pp. 793-798, 2008.

[6] C. Delacourt, M. Safari, "Life simulation of a graphite/$LiFePO_4$ cell under cycling and storage," Journal of The Electrochemical Society, vol. 159, pp. A1283-A1291, 2012.

[7] A.P. Schmidt, M. Bitzer, Á.W. Imre, "Guzzella, L. Model-based distinction and quantification of capacity loss and rate capability fade in Li-ion batteries," Journal of Power Sources, vol. 195, pp. 7634-7638, 2010.

[8] R. Fu, S.Y. Choe, V. Agubra, J. Fergus, "Modeling of degradation effects considering side reactions for a pouch type Li-ion polymer battery with carbon anode," Journal of Power Sources, vol. 261, pp. 120-135, 2014.

[9] M. Doyle, T.F. Fuller, J. Newman, "Modeling of galvanostatic charge and discharge of the lithium/polymer/insertion cell," Journal of The Electrochemical Society, vol. 140, pp. 1526-1533, 1993.

[10] M. Doyle, J. Newman, A.S. Gozdz, C.N. Schmutz, J.M. Tarascon, "Comparison of modeling predictions with experimental data from plastic lithium ion cells," Journal of The Electrochemical Society, vol. 143, pp. 1890-1903, 1996.

[11] M. Guo, G. Sikha, R.E. White, "Single-particle model for a lithium-ion cell: Thermal behavior," Journal of The Electrochemical Society, vol. 158, pp. A122-A132, 2011.

[12] L. Zhang, L. Wang, C. Lyu, J. Li, J. Zheng, "Non-Destructive Analysis of Degradation Mechanisms in Cycle-Aged Graphite/$LiCoO_2$ Batteries" Energies, vol. 7, No. 10, pp. 6282-6305, 2014.

[13] S.J. Drake, D.A. Wetz, J.K. Ostanek, S.P. Miller, J.M. Heinzel, A. Jain, "Measurement of anisotropic thermophysical properties of cylindrical Li-ion cells," Journal of Power Sources, vol. 252, pp. 298-304, 2014.

[14] L. Zhang, L. Wang, C. Lyu, J. Zheng, F. Li, "Multi-physics modeling of Lithium-ion batteries and charging optimization," IEEE PHM Conference, pp. 391-400, August 2014.

[15] L. Zhang, C. Lyu, L. Wang, J. Zheng, W. Luo, K. Ma, "Parallelized Genetic Identification of the Thermal-Electrochemical Model for Lithium-Ion Battery," Advances in Mechanical Engineering, Vol. 2013, Article ID 754653, pp. 1-12, 2013.

[16] L. Zhang, L. Wang, G. Hinds, C. Lyu, J. Zheng, J. Li, "Multi-objective optimization of lithium-ion battery model using genetic algorithm approach," Journal of Power Sources, Vol. 270, pp. 367-378, 2014.